



Research Article

Silver Tin Copper (Ag-Sn-Cu) Powder Coating on Aluminum Substrate and Teeth Using High Pressure Cold Spray

Syed Roohullah Jan¹, Kareem Akhtar^{2*}, Uroosa¹, Muhammad Zeeshan Zahir³, Abdul Shakoor⁴

¹Mechanical Engineering UBC, Vancouver, Canada; ²ESM, Virginia Tech, Blacksburg Virginia, USA; ³School of Mechanical Engineering, Hanyang University, Seoul, Republic of Korea; ⁴Department of Materials, Loughborough University, Loughborough, UK.

Abstract: Coatings generated using traditional methods undergo oxidation and contamination problems. Cold spray is recently used to obtain pure coatings without oxidation. In this work coatings of Ag-Sn-Cu powder are achieved on the Aluminum substrate and human teeth, using the high-pressure cold spray technique. The powder when mixed with Mercury is called amalgam and is commonly used in dental applications for cavity filling. However, Mercury is health hazardous. In the present study coating of Ag-Sn-Cu is achieved through cold spray without adding mercury. The particle size and morphology of Ag-Sn-Cu powder are studied, before and after coatings. Hardness tests are carried out to determine surface hardness before and after the coatings. This study reveals that uniform composite coating of Ag-Sn-Cu can be achieved without Mercury using the cold spray. Hence cold spray technique can be used in the future for filling cavities and other dental applications.

Received: February 08, 2023; **Accepted:** October 18, 2023; **Published:** November 25, 2023

***Correspondence:** Kareem Akhtar, ESM, Virginia Tech, Blacksburg Virginia, USA; **Email:** kareemakhtar@uetpeshawar.edu.pk

Citation: Jan, S.R., Akhtar, K., Uroosa, M.Z. Zahir, A. Shakoor. 2023. Silver tin copper (Ag-Sn-Cu) powder coating on aluminum substrate and teeth using high pressure cold spray. *Journal of Engineering and Applied Sciences*, 42: 19-30.

DOI: <https://dx.doi.org/10.17582/journal.jeas/42.1.19.30>

Keywords: Ag-Sn-Cu powder, Dental cavity filling, Coating, cold spray, Surface treatment



Copyright: 2023 by the authors. Licensee ResearchersLinks Ltd, England, UK.

This article is an open access article distributed under the terms and conditions of the Creative Commons Attribution (CC BY) license (<https://creativecommons.org/licenses/by/4.0/>).

Introduction

Teeth are essential and highly utilized components of the human body, consisting of the outermost layer called enamel, followed by dentine, and the innermost pulp containing blood vessels and neurons. If teeth are not cleaned daily, food deposits on their surface and causes bacteria to grow on the tooth's upper layer, leading to decay that can continue until the enamel is eroded. This process, depicted in Figure 1, exposes the dentine, causing pain during further decay.

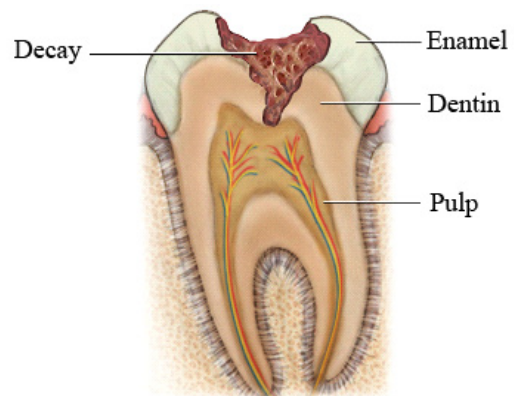


Figure 1: Dental decay process (Grewal, 2016).

When treating dental decay, the dentist removes the affected part of the tooth using compressed air and other tools, which may also remove some healthy parts of the tooth to create a cavity for filling, as shown in Figure 2 (Laudenbach, 2014).

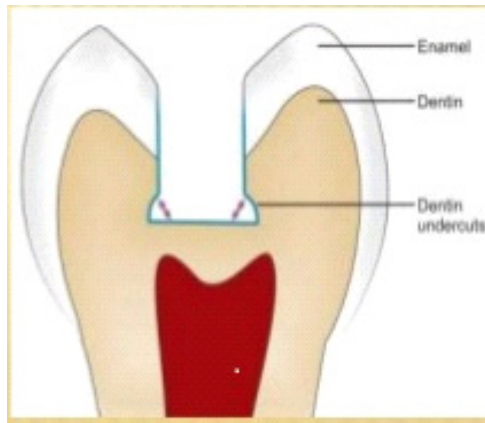


Figure 2: Cavity made in the tooth for amalgam fillings. (Laudenbach, 2014).

Enamel is composed of 96% inorganic material and 4% organic material and water (by weight). Dentine, on the other hand, contains 70% inorganic material. The inorganic material primarily consists of calcium phosphate $\text{Ca}_{10}(\text{PO}_4)_6 \cdot 2(\text{OH})_1$, with traces of other elements including Na, Cl, and Mg₂ are also present. Dental amalgam is created by mixing alloy powder of silver, copper, and tin with liquid mercury in a 1:1 ratio. The alloy powder contains a relative amount of Ag (40-70%), Cu (2-40%), and Sn (25-29%). Zinc may also be added as a scavenger, as it is lost in the form of oxides during melting. Silver (Ag) provides color and increases strength and expansion during setting. It also minimizes amalgam flow and reduces the creep phenomenon. Tin (Sn) minimizes corrosion, optimizes reaction time and expansion, and controls the reaction of mercury with silver. The addition of copper (Cu) increases strength, hardness, and setting expansion (Davis, 2004).

Amalgam in teeth slowly gains strength and takes 24 hours to reach its full strength. It also expands about 0.1% over a 6-8 hour period. Therefore, patients who have received amalgam fillings are instructed to avoid applying large stress until the filling has reached its full strength (Brodji *et al.*, 1996).

Mercury intake is highly hazardous, with about 80% of it being absorbed into the bloodstream through the lungs. It can cause severe damage to human organs, including the kidneys, digestive, respiratory, immune,

and nervous systems. Mercury exposure can lead to various health effects such as vision and hearing problems, paralysis, tremors, insomnia, lack of attention and emotional instability, and developmental defects during fetal and childhood stages.

Due to the numerous health hazards posed by mercury, the World Health Organization (WHO) and the United Nations Environmental Programme (UNEP) held a meeting in 2009 to investigate the effects of mercury from the dental sector on the environment and human health. Their aim was to devise strategies for reducing mercury contamination.

In 2017, the US Environmental Protection Agency (EPA) presented guidelines that limit dental practices from draining dental amalgam to the ground. Table 1 presented by UNEP shows the disposition of mercury resulting from the use of amalgam in dental applications (WHO, 2009).

Table 1: Mercury disposal due to dental amalgam (WHO, 2009).

Source	Mercury (metric Ton/Yr)
Atmosphere	50-70
Surface water	35-45
Ground water	20-25
Soil	75-100
Recycling of amalgam	40-50
secure disposal	40-50
Total	260-340

Aluminum is an important metal and is abundantly found in nature. It was used as a base material in this study, and it makes up about 8.23% of the Earth's crust. Due to its lightweight and high strength/weight ratio, aluminum has many engineering applications. Compared to steel, it is three times lighter but has about the same stiffness. However, the main problem with aluminum is its oxidation when exposed to air, which forms a non-ductile and electrical insulating layer of oxide (Al_2O_3) on its surface. This oxide layer has a preventive effect on further oxidation, but aluminum alloys are more susceptible to this oxidation than their pure form (Makeitfrom, 2009).

Boissonnet *et al.* (2019) worked on the mechanisms of formation on pure nickel of full thermal barrier coating systems, aluminide coating, thermally grown oxide and thermal barrier top coating. Zeng *et al.* (2020) explored the biocompatibility and cell growth

of a Ti-Ta composite coating made from solid state cold spraying deposition. [Omar et al. \(2021\)](#) studied, TiO₂ coatings deposition on copper and aluminum substrates and the adhesion strength was evaluated to investigate the bonding mechanism. The influence of substrate hardness and remaining surface oxide layer was investigated by annealing the substrates with various temperatures. [Lopes-Pirize et al. \(2022\)](#) developed a new multifunctional zirconia-ceria/alumina (Ce-TZP/Al₂O₃) composite with an antimicrobial glass-based coating to be used in multi-unit abutments compatible with commercially available Ti implants for peri-implantitis prevention. An airbrush spraying technique was applied to coat the sintered ceramic composite starting from a glass powder suspension.

There are several coating methods available, but they all have certain drawbacks. For instance, many of them require high temperatures to melt the coating material, which makes them more susceptible to oxidation problems. Furthermore, these methods cannot be used with temperature-sensitive materials, either as coating materials or base materials. In addition, they are often time-consuming and expensive.

This study utilizes a relatively new technique called cold spray coating. As the name implies, this technique creates the coating at room temperature, without melting the particles or substrate. There are two types of cold spray: low-pressure cold spray (LPCS) and high-pressure cold spray (HPCS), which differ in how the powder enters the nozzle from the powder chamber.

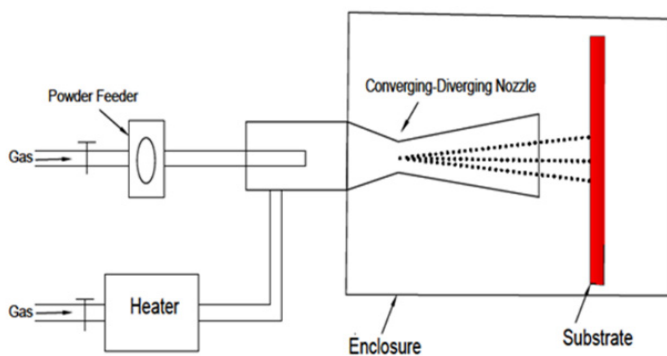


Figure 3: Operational principle of high-pressure cold spray ([Akhtar, 2015](#)).

In the HPCS process, the powder particles are introduced into the nozzle at high pressure, before the converging part of the nozzle ([Alkhimov et al., 1994](#)). As shown in [Figure 3](#), the nozzle can use air

or inert gases such as helium and nitrogen as carrier gases. The particle velocity depends on the velocity of the gas, which carries the powder during expansion in the nozzle ([Singh et al., 2012](#)). At the nozzle exit, the powder achieves supersonic speed.

In low-pressure cold spray (LPCS), the powder is injected into a low-pressure expanding gas in the diverging section of the nozzle, as shown in [Figure 4](#). The pressure in the powder chamber in LPCS is also relatively low compared to high-pressure cold spray (HPCS) ([Kashirin et al., 2002](#)).

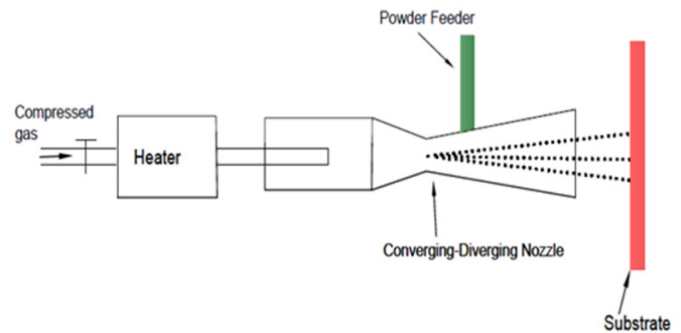


Figure 4: Operational principle of low-pressure cold spray ([Akhtar, 2015](#)).

High-pressure cold spray (HPCS) provides higher coating efficiency compared to low-pressure cold spray (LPCS), but it is an expensive method and has a short nozzle life. HPCS is used to generate zinc coatings using aluminum as the base material. The working principle of HPCS is that the kinetic energy of particles causes them to undergo permanent shear deformation upon striking the base material, resulting in adiabatic shear deformation due to abrupt colliding. This produces stresses greater than the yield stresses, and both particles and substrate undergo shear straining ([Assadi et al., 2003](#); [Klinkov et al., 2005](#); [Bae et al., 2008](#); [Li et al., 2009](#); [Spencer et al., 2010](#); [Spencer et al., 2010](#)). If there is surface oxide, it breaks down due to high straining, allowing for metallic contact ([Grujicic et al., 2004](#)).

When a high-velocity gas jet interacts with the one bouncing back from a substrate, a pressure zone in the gas flow field called a “bow shock” develops ([Kosarve et al., 2001](#); [Papyrin et al., 2007](#)). Only those particles that pass through a high-pressure region and still retain their critical velocity can deposit successfully. The critical velocity for zinc metal is calculated to be above 350 m/sec ([Schmidt et al., 2006](#)).

Materials and Methods

Ag-Sn-Cu particles size investigation

A laser particle size analyzer (Horiba LA-920) was used to determine particle sizes in the dispersion medium of ethanol. The results of the test are shown in Figure 5, which displays the particle diameter on the x-axis with percent weight volume on the left axis and percent cumulative volume on the right axis. Particle diameter ranges from 1 μ m-500 μ m, and the corresponding percent weight volume can be read from the left axis for each range of particle size distribution.

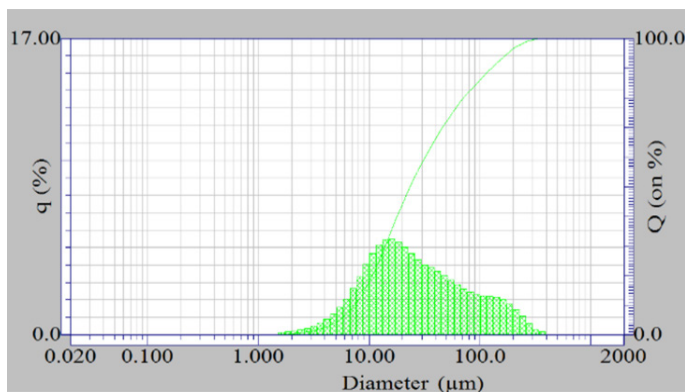


Figure 5: Particle size distribution by laser-particle size analyzer (LA-920).

AG-Sn-Cu powder morphology

The morphology of the powder plays a vital role in the particle velocity during its flight. Particle morphology was investigated by performing scanning electron microscopy of the AG-Sn-Cu powder sample, and the results are presented in Figure 6. It can be observed that the powder sample has irregular particle morphology, and the particle size ranges from approximately 1 μ m-500 μ m, as observed in the laser particle analyzer shown in Figure 5. The test was performed using an electron microscope at 15 KV, and the particle morphology is presented more clearly at higher magnifications of 250X and 500X in Figure 6B, C, respectively.

Composition of Ag-Sn-Cu alloy-powder

The powder was received with an average composition of Ag (45%) - Sn (30%) - Cu (25%) according to the company claim. The actual alloy powder, which is in gray color, is also shown in Figure 7A. The powder's composition was investigated using the EDX test, and both the elemental percent composition and the elemental peaks are presented in Figure 7B. The study found that the investigated composition of the alloy

was Ag (43.38%) - Sn (34.03%) - Cu (22.59%), with no other impurities found in the powder. Therefore, the powder was considered to have a pure composition.

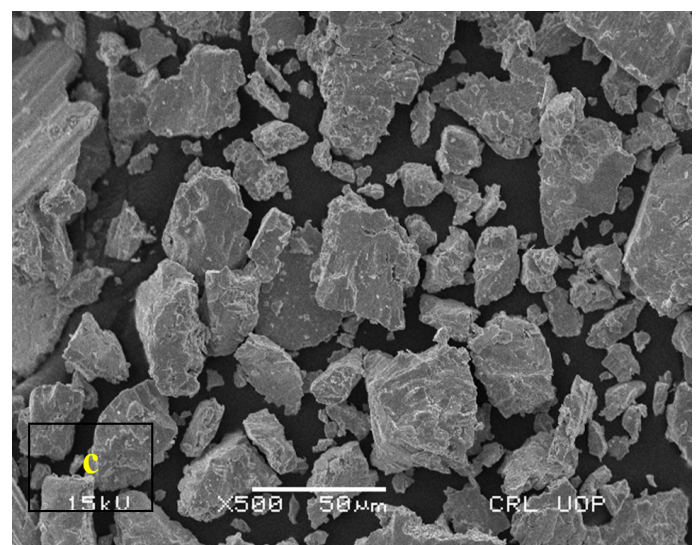
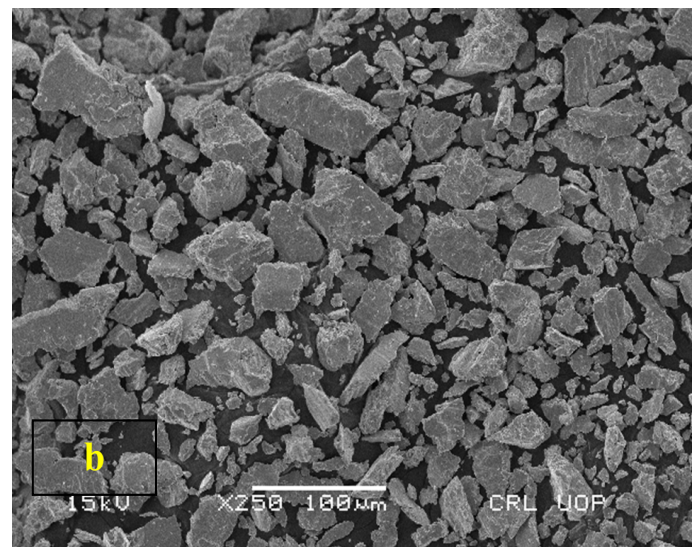
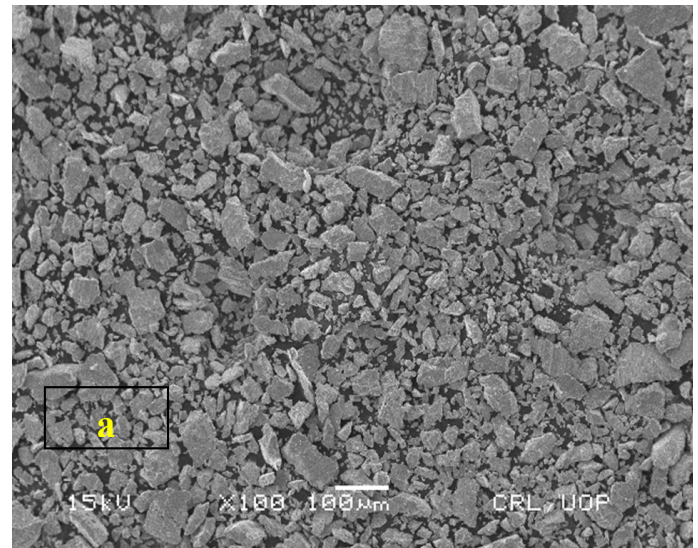
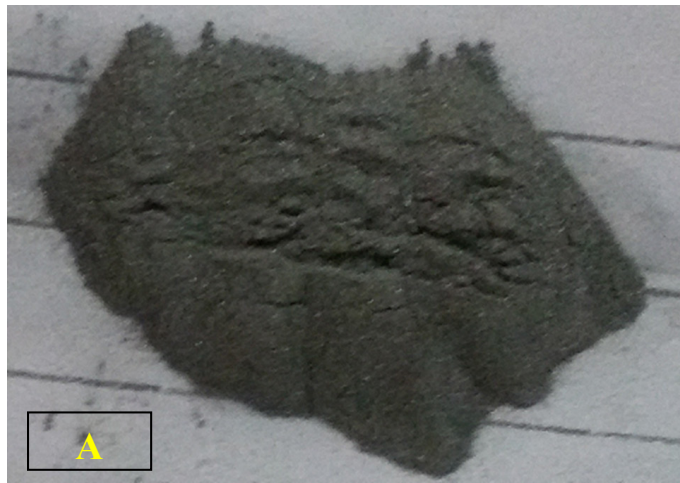


Figure 6: Scanning electron microscopy (SEM) images of Ag-Sn-Cu alloy-powder at different magnifications: (a) 100 X (b) 250X (c) 500X



Element	Weight%	Atomic%
Cu L	22.59	34.04
Ag L	43.38	38.51
Sn L	34.03	27.45
Totals	100.00	

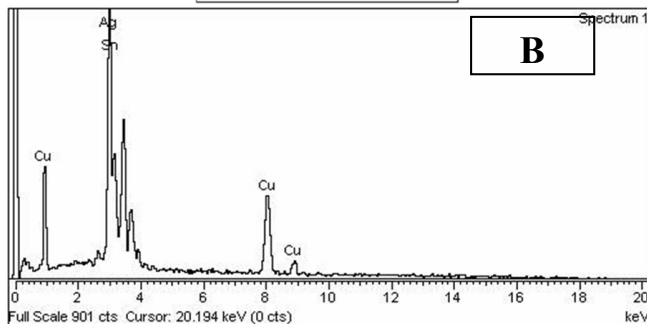


Figure 7: (A) Ag-Sn-Cu alloy-powder, (B) EDX of alloy-powder.

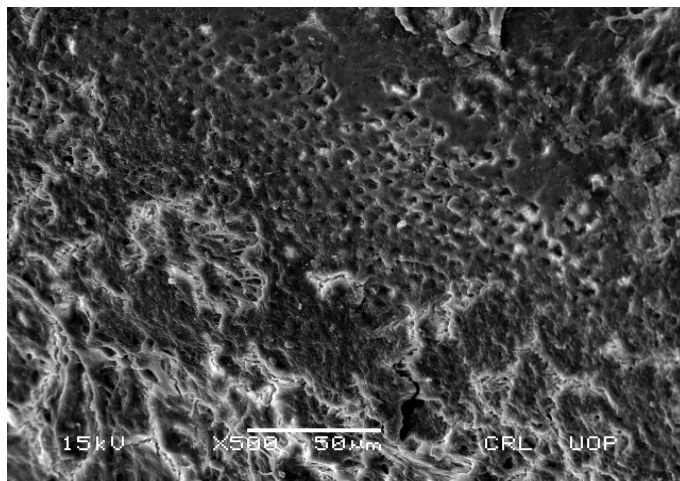


Figure 8: SEM image of Teeth before cavity at 500 X magnification.

Tooth characterization before coating

Figure 8 shows an image of the uncoated tooth. The tooth enamel was studied with X-ray energy spectroscopy at 500X magnification and 15 KV. To create a cavity in the tooth, a dental instrument was used, and the resulting cavity is shown in Figure 9 at

1,000X magnification and 15 KV. The cavity-making process is similar to the one used for the tooth filling with amalgam, but in this study, the cold spraying technique will be used to fill the cavity to avoid mercury inhalation and provide just-in-time service.

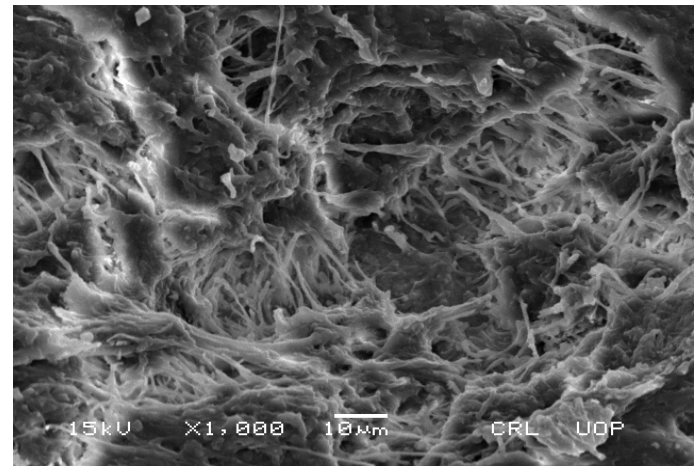


Figure 9: SEM image of cavity made by dental instruments at 1,000X magnification.

Aluminum substrate surface characteristics

To investigate the effect of the alloy powder (Ag-Sn-Cu) coating on teeth and aluminum substrate, we examined the coating's impact on hardness, coating strength, and other surface properties. We used pure aluminum material of grade 1100 H14, with a sheet thickness of 1.5 mm, and cleaned it of surface impurities through rough polishing. To accomplish this, we used a polishing wheel with grid paper 180. After the polishing operation, we studied the surface texture using an optical microscope at 5X magnification. Figure 10 shows the results, where we can observe the effect of polishing in the form of remaining surface scratches.

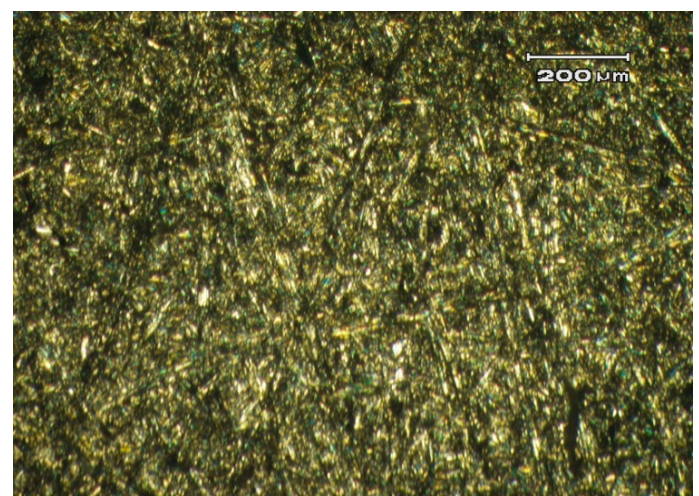


Figure 10: Optical microscope image of Aluminum substrate surface at 5X magnification.

Elemental composition of the substrate

The composition of the tooth was discussed in the literature review of this work, as investigated in previous studies. To determine the composition of the aluminum substrate, energy dispersive X-ray spectroscopy (EDX) was used, and the results are shown in Figure 11, which presents the elemental percent composition and relevant compositional peaks.

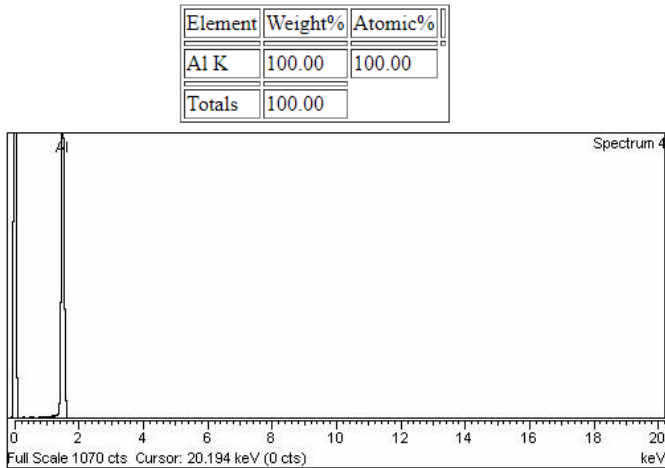


Figure 11: EDX and percent composition of the Aluminum substrate.

Sample preparation

Ag-Sn-Cu alloy powder was deposited on the actual tooth, while samples of the aluminum substrate were prepared for the characterization study. To prepare the substrate samples, the aluminum sheet was first polished and then cut into small pieces using a specialized sheet-cutting machine capable of producing strips down to a millimeter in size. Pieces with equal dimensions of 5mm x 10mm were prepared to ensure uniformity and facilitate the characterization study of the coating due to the small sample size. This approach aimed to preserve the coating in its original form. The sectioned substrate samples without any coating are presented in Figure 12.



Figure 12: Sectioned specimen.

Experimental setup

A two-stage air compressor with an inter-cooler is used to perform the cold spraying process and achieve a stagnation pressure of 14 bars at room temperature. The experimental setup is shown in Figure 13, which included a two-stage compressor with a water inter-cooler that was used to build up the pressure to 14 bars in a storage cylinder. Air was drawn from the atmosphere and purified using an air filter to remove dust and moisture before being fed to the supersonic nozzle along with high-pressure air from the storage tank. The powder was also introduced into the convergent part of the nozzle. To facilitate the smooth flow of powder particles and prevent backflow, the powder chamber was kept at a higher pressure than the nozzle inlet.

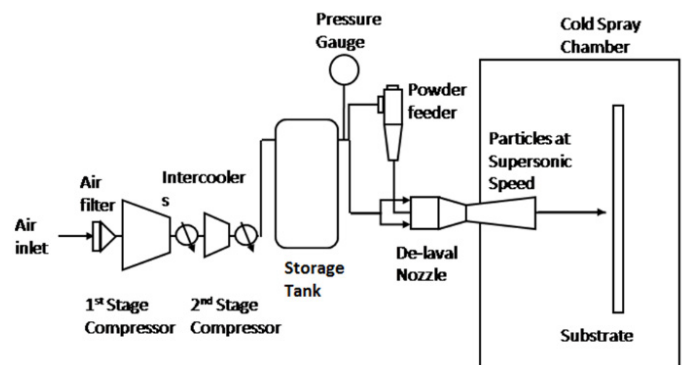


Figure 13: Schematic diagram of cold spray.

The cold spraying process was carried out in a spray chamber where a high-speed air jet containing powder particles was impacted on a substrate from the nozzle, which was manually given to and fro motion during the spray. The substrate was fixed at a right angle to the nozzle, with the nozzle-to-substrate distance varying between 10 mm and 60 mm approximately. The substrate was placed on a stage that moved up and down at 50 mm/sec through a DC motor. Thick Ag-Sn-Cu coating was achieved through multiple repetitions of the nozzle.

To achieve an isobaric jet, a special type of convergent-divergent (De-laval) nozzle was used. The design parameters of the nozzle can be found in Table 2. The nozzle was designed in two parts, the converging part with a throat section and the diverging part. The throat section has a uniform diameter to prevent sudden gas expansion inside the nozzle and turbulence in the expanding gas flow. The external threads on the throat section allowed for easy assembly with the eternal diverging section. The inlet diameter of the nozzle

was 8.92 mm, the throat diameter was 2mm, and the outlet diameter was 2.79mm, as shown in the CAD model in Figure 14 and the nozzle assembly in Figure 15.

Table 2: Cold spray nozzle design parameters.

S. No	Nozzle parts	Dimensions
1.	Inlet diameter (D_{In})	8.97mm
2.	Throat diameter (D_{Th})	2 mm
3.	Exit diameter (D_{Ex})	2.92 mm
4.	Convergent length (L_C)	60 mm
5.	Divergent length (L_D)	140 mm
6.	Throat length (L_{Th})	5 mm
7.	Total length (L_T)	205 mm
8.	Exit Mach number (Me)	1.62

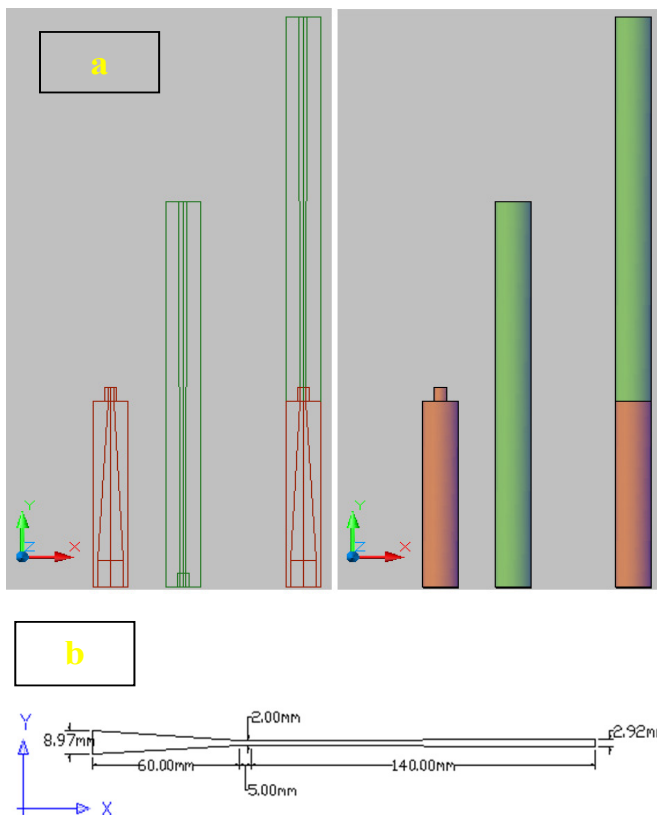


Figure 14: CAD model of cold spray nozzle: (a) 3-D (b) 2-D.



Figure 15: Cold spray nozzle.



Figure 16: Cold spray gun.

The assembled gun, along with the attached powder feeder, is also shown in Figure 16. The powder chamber was attached and inclined at an angle of 60 degrees to the nozzle, adding a gravitational effect to the powder. A DC motor with a screw shaft (worm mechanism) was installed on the powder chamber, which carried the powder for feeding into the nozzle at a uniform rate. The worm shaft extended into a 2mm hole at the bottom of the powder chamber, carrying the powder during the spraying process and dropping it at the inlet of the converging part of the nozzle. This mechanism helped to generate coatings of uniform thickness, provided the substrate and nozzle had a constant-rate displacement. It also prevented the nozzle and powder chamber from blocking.

Results and Discussion

Optical microscope characterization of the coated surface
 The designed cold spray facility was used to produce an Ag-Sn-Cu alloy-powder coating at room temperature with a stagnation pressure of 14 Bars. Figure 17 shows the uncoated and coated Aluminum base material alongside the Ag-Sn-Cu alloy-powder coating. The results indicate that the substrate was completely covered by the Ag-Sn-Cu alloy-powder coating.

To observe details invisible to the naked eye, optical microscopy was performed on the Ag-Sn-Cu alloy-powder coating. The study utilized an optical microscope that works by reflecting light. The results are displayed in Figure 18, which shows that the coating is continuous and dense when observed at 5X and 10X magnifications. Additionally, the variation in color shade is evidence of a solid-state coating with a rough surface profile.



Figure 17: Aluminum substrate before and after coating.

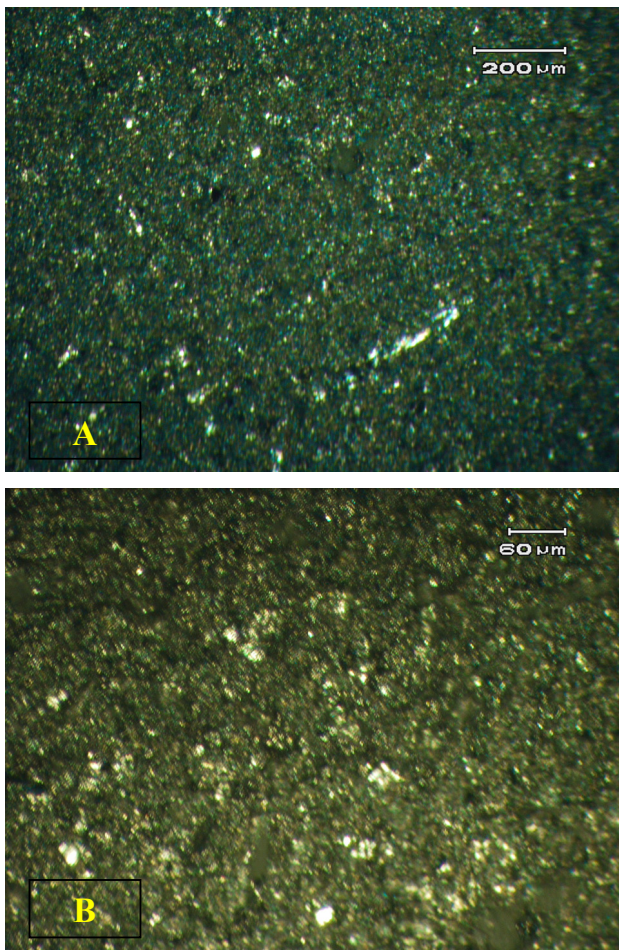


Figure 18: Optical microscope image at different magnifications (A) 5X-magnified, (B) 20X-magnified.

Scanning electron microscopy (SEM) of the coated surface
 An SEM study was conducted on both the tooth and Aluminum substrate after coating. **Figure 19A** shows the tooth with Ag-Sn-Cu coating at 20X magnification and 15 kv. The image displays that the tooth cavity is filled with solid-state metallic powder, resulting in a successive metallic layer on the affected tooth part. The cavity is also partially filled with solid-state alloy powder. **Figure 19B, C**, viewed at higher magnifications of 30X and 50X, respectively, reveal further details of the coated tooth. A dense metallic layer has developed on the tooth's surface, demonstrating that cold spray can be applied effectively for tooth fillings without using hazardous mercury.

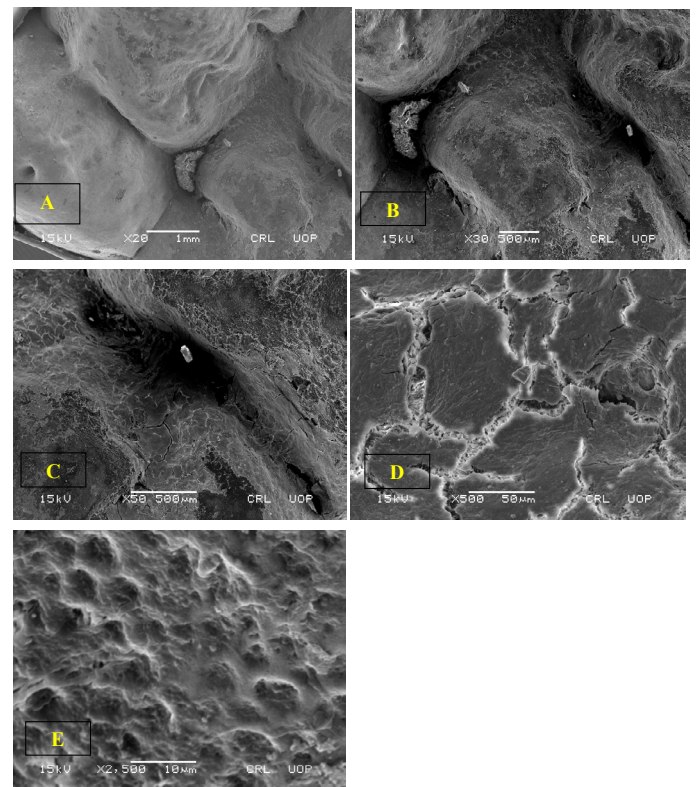


Figure 19: SEM image of the coated tooth at different magnifications and 15 kv, (A) 20 X, (B) 30 X, (C) 50 X, (D) 500X, (E) 2500X.

The coating is shown at a much higher magnification of 500X and 15 kv in **Figure 19D**. The image captures the solid-state coating process as each particle undergoes plastic deformation upon impact with the tooth surface. The coating fracture is a result of the solid-state coating process. **Figure 19E** displays the coating at a further magnification of 2500X and 15kv. The image showcases a uniform and continuous coating on the tooth surface with no voids present. This void-free coating indicates that bulk coating can be achieved.

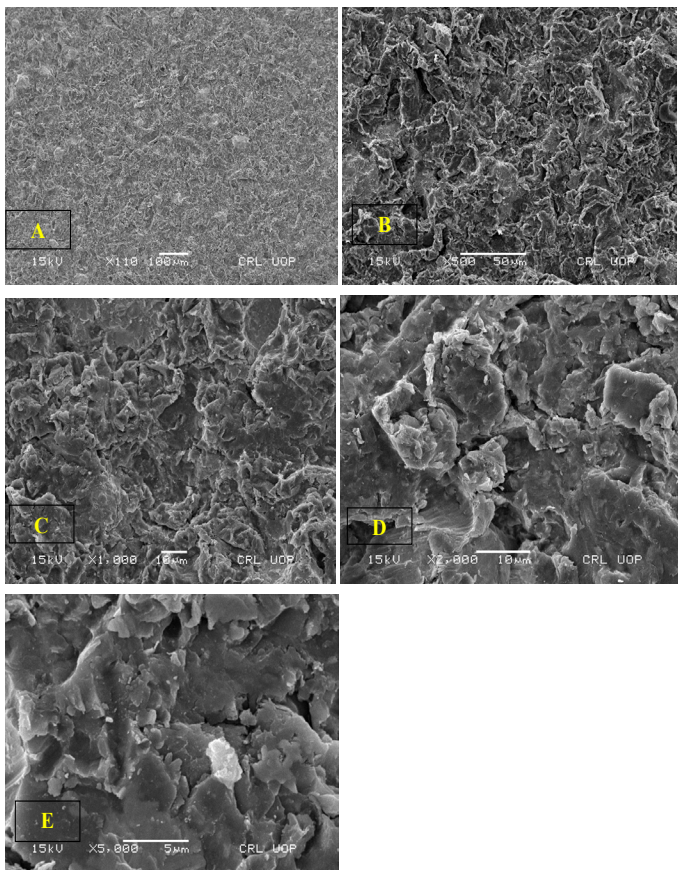


Figure 20: Scanning electron microscope (SEM) images of coated Aluminum surface at different magnifications, (A) at 110X, (B) at 500X, (C) 1000X, (D) 2000X, (E) 5000X.

SEM images of the coated aluminum substrate at different magnifications are also presented in Figure 20. Figure 20A shows a continuous and dense coating, with no voids or uncoated regions visible. The particles are well-bonded, indicating that the coating was generated due to severe particle deformation of the Ag-Sn-Cu alloy powder. The solid-state coating process is also evident at higher magnifications of 500X and 1000X in Figure 20B, C, respectively. The impact of particles leads to adiabatic shear deformation, resulting in a cup-shaped surface profile of the coatings. The particles transform into a continuous coating with their actual composition, and no loosely bonded particles of alloy powder are found in the coating. The coatings at even higher magnifications of 2000X and 5000X are shown in Figure 20D, E, respectively. The ductile behavior of the Ag-Sn-Cu alloy powder is also evident, with no visible brittle fractures of the particles. The lateral deformation of particles on impact with the surface results in sharp nooks, and during this process, the particles also splatter onto the coating surface, which can be observed at higher magnification.

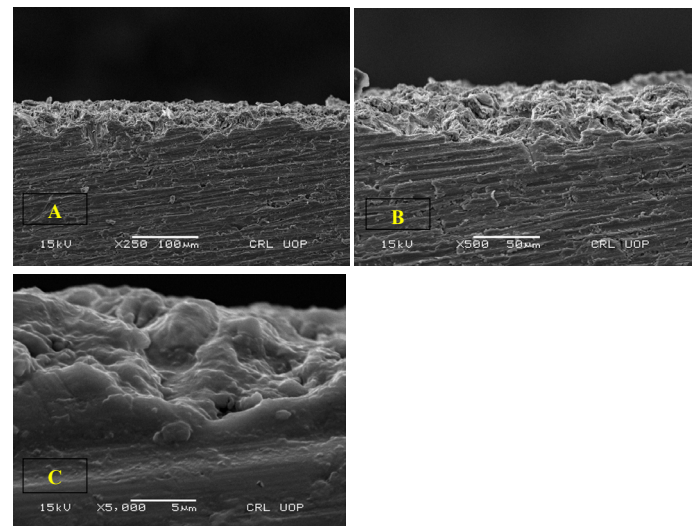


Figure 21: Scanning electron microscope image of coating cross-sections (A) 250 X, (B) 500X, (C) 5000X.

Electron microscopy was also employed to investigate the cross-section of the coating on the Aluminum substrate. The cross-sectional surface was first polished, and the SEM images of the cross-section are presented in Figure 21. In Figure 21A, it is apparent that a 5-micron thick coating has been achieved, which demonstrates good bonding with the substrate, as seen in Figure 21B. The coating cross-section is further shown at 5000X magnification in Figure 21C. No voids can be observed in the coating, and all the particles are well bonded with good adhesion between the coating and the substrate.

Coating composition

Following the successful application of coatings onto the substrate, their composition was analyzed to determine whether any changes in their phase had occurred. Electron dispersive X-ray spectroscopy (EDX) was employed to investigate the elemental composition, and the results are presented in Figure 22, which includes both the elemental percent composition and the elemental peaks. The analysis reveals that the coating has remained in its original form without any phase change. All of the elements of the alloy powder are present in their actual form and relative percentages. It is worth noting that the elemental peak for gold (Au) in Figure 22 is a result of the surface preparation for SEM study by coating it with gold to increase surface conductivity.

Hardness test

In the cold spray process, the base material and the coating material (in powder form) are both treated at room temperature. As a result, the hardness of the

base material is expected to increase. To investigate the effect of coating Ag-Sn-Cu alloy powder on the hardness of the Aluminum substrate, a micro-Vickers hardness test apparatus was used. The test was performed on the substrate before and after the coating process, using a load of 15 grams on the sample and a dwell time of 10 seconds. The results are presented in Figure 23, which shows that the hardness value of the uncoated aluminum substrate has an average scale of 25.78 Hv0.1/15, while the hardness value of the coated aluminum sample has an average scale of 37.43 Hv0.1/15, indicating a more than 45% increase in hardness. This increase in hardness is attributed to the good bonding of the particles due to solid-state adhesion.

Element	Weight%	Atomic%
Cu L	19.63	14.33
Ag L	38.70	68.79
Sn L	29.98	13.38
Au M	11.69	3.50
Totals	100.00	

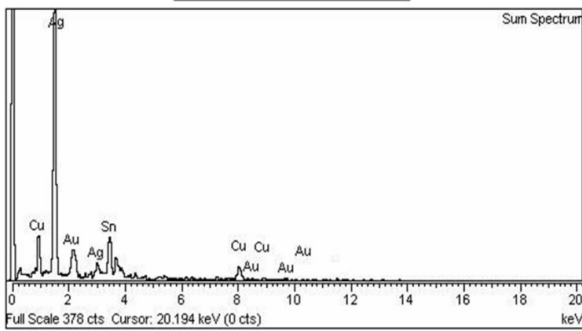


Figure 22: Energy dispersive x-ray spectroscopy (EDX) of the coating.

Surface roughness

For this study, we selected large particle-sized Ag-Sn-Cu alloy powder ranging from 1 to 500 microns in an irregular shape. We investigated its impact on the coating surface profile using the Metituyo optical surface stylus-meter Model SJ-400, following ISO 1997 standards. The figure demonstrates that the surface roughness (Ra) increased from 0.22 microns to 0.28 microns.

Coating efficiency

In many thermal spray processes, a certain proportion of the sprayed material will rebound or splash off the surface rather than being ‘captured’ in the coating, resulting in a process efficiency lower than 100%. Thus, the term deposition efficiency (DE) has come into use and is defined according to Equation 1 (King et al., 2015).

$$DE = \frac{\Delta m}{M_0} \dots (1)$$

where Δm is the increase in weight of the sample during spray, and M_0 is the total mass of material fired at the sample. To determine the amount of Ag-Sn-Cu (by mass) on the aluminum substrate, we calculated the coating efficiency. We conducted three different experiments where we measured a weighted amount

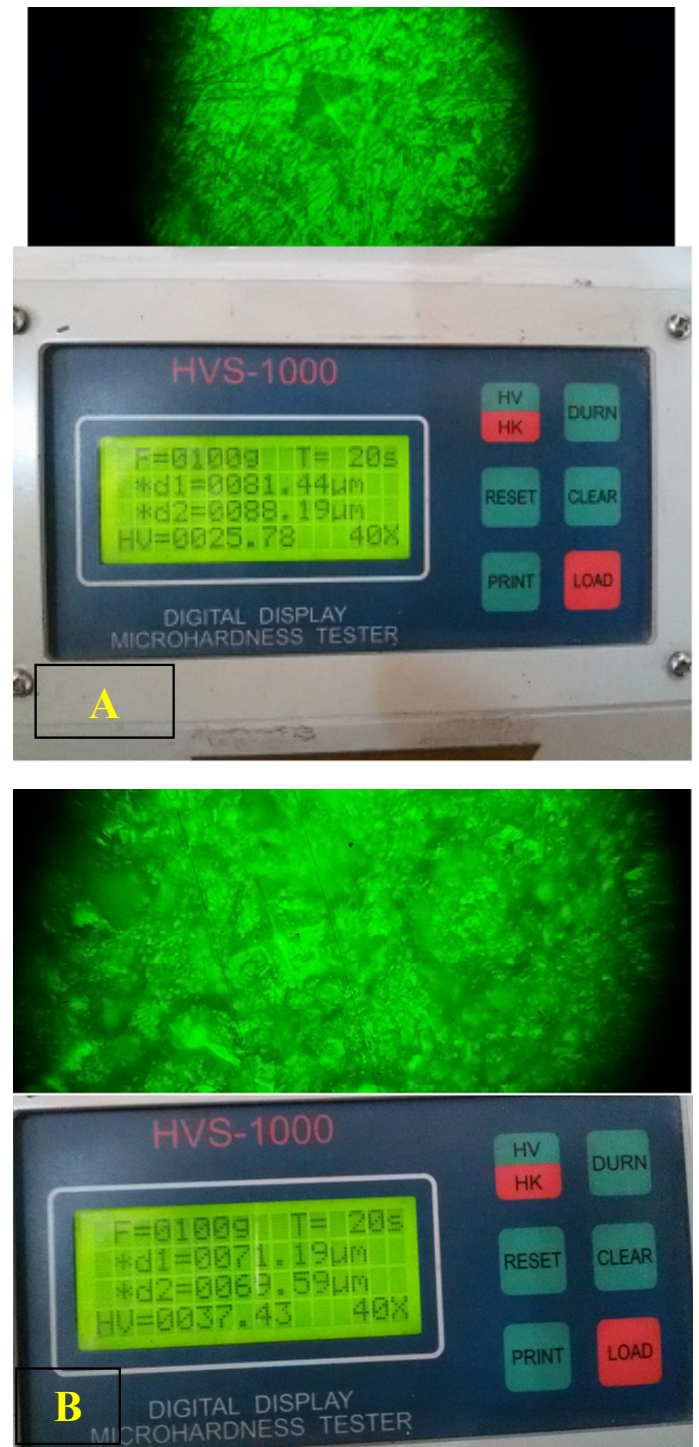


Figure 23: Micro-hardness test of, (A) Aluminum substrate, (B) Ag-Sn-Cu alloy powder coating on an aluminum ally.

of Ag-Sn-Cu before coating. We also weighed the substrate. Then, we performed the cold-spray coating and weighed the coated substrate again. The increase in weight indicated the amount of coated powder. The results showed an average of 78.744% of Ag-Sn-Cu powder was coated. The calculated efficiency is shown below.

$$\begin{aligned} \text{Base-Material} &= \text{Tooth/Aluminum} \\ \text{Metallic Powder} &= \text{Ag-Sn-Cu} \\ \text{Amount of Ag-Sn-Cu powder} &= 27.423 \text{ g} \\ \text{Amount of base-Material} &= 31.255 \text{ g} \\ \text{Amount of coated substrate} &= 52.849 \text{ g} \\ \text{Stagnation Pressure} &= 14 \text{ bar} \\ \text{Nozzle-Standoff distance} &= 60 \text{ mm} \\ \text{Amount of deposited powder} &= \text{“Amount of coated-} \\ &\text{substrate”} - \text{“amount of un-coated substrate”} = \\ &52.849 \text{ g} - 31.255 \text{ g} = 21.594 \text{ g} \\ \text{The efficiency of coating} &= (21.594/27.423) * 100 = \\ &78.744 \%. \end{aligned}$$

Conclusions and Recommendation

This study demonstrated that Ag-Sn-Cu alloy powder coatings can be successfully generated on teeth and aluminum substrates using cold spray technology. SEM studies of the coatings showed well-bonded Ag-Sn-Cu alloy particles in the form of a continuous and thick coating with a void-free interface between the coating and substrate. A cross-sectional SEM study of the coating revealed that a 5-micron coating thickness was achieved. The thick coating is a result of solid-state plastic deformation of the alloy particles, which suggests that the cold spray technique can be used to generate even thicker coatings.

However, the surface roughness increased slightly due to the deposition of particles in solid form. The Ag-Sn-Cu coatings were made possible by a nozzle that accelerated the particles above the critical velocity. The successful deposition of the coating indicated that the critical velocity of Ag-Sn-Cu was achieved, and the designed nozzle was supersonic.

Based on these findings, we concluded that cold spray coating technology can be successfully used for dental filling applications without using mercury.

Acknowledgement

Authors extend their sincere appreciation to the

Department of Mechanical Engineering, UET Peshawar for generously providing the necessary experimental facilities crucial for the completion of this research work.

Author's Contribution

Conceptualization: Kareem Akhtar and Abdul Shakoor;
Methodology: Muhammad Zeeshan Zahir, Uroosa and Kareem Akhtar;
Validation: Abdul Shakoor and Uroosa;
Investigation: Syed Roohullah Jan;
Writing—original draft preparation: Syed Roohullah Jan and Muhammad Zeeshan Zahir;
writing—review and editing: Syed Roohullah Jan, Kareem AKhtar and Muhammad Zeeshan Zahir.

Conflict of interest

The authors have declared no conflict of interest.

References

- Akhtar, K., 2015. A numerical study of supersonic rectangular jet impingement and applications to cold spray technology. PhD thesis, Virginia Tech University, Blacksburg, USA
- Alkhimov, A.P., A.N. Papyrin, V.F. Kosarev, N.L. Nesterovich and M.M. Shushpanov. 1994. Gas-dynamic spraying method for applying a coating, in U.S. Patent, 5: 302-414.
- Assadi, H., F. Gartner, T. Stoltenhoff and H. Kreye. 2003. Bonding mechanism in cold gas spraying. *Acta Mater.*, 51: 4379-4394. [https://doi.org/10.1016/S1359-6454\(03\)00274-X](https://doi.org/10.1016/S1359-6454(03)00274-X)
- Bae, G., Y. Xiong, S. Kumar, K. Kang and C. Lee. 2008. General aspects of interface bonding in kinetic sprayed coatings. *Acta Mater.*, 56: 4858-4868. <https://doi.org/10.1016/j.actamat.2008.06.003>
- Benjamin, G.B., G. Gilles, B. Fernando and Pedraza. 2019. Development of thermal barrier coating systems from Al microparticles. Part I: Influence of processing conditions on the mechanisms of formation. December 2019, Volume 380 (Issue Complete), *Surface and Coatings Technology*. <https://doi.org/10.1016/j.surfcoat.2019.125085>
- Boissonnet, G., B. GrÃ©goire, G. Bonnet, F. Pedraza. 2019. Development of thermal barrier coating systems from al microparticles. Part

- i: Influence of processing conditions on the mechanisms of formation. *Surface and Coatings Technology*, 380:125085. <https://doi.org/10.1016/j.surfcoat.2019.125085>
- Bordji, K., J.Y.J.D. Mainard, E. Payan, P. Netter, K.T. Rie, T. Stucky and M. Hage-Ali. 1996. *Biomaterials*, 17: 929. [https://doi.org/10.1016/0142-9612\(96\)83289-3](https://doi.org/10.1016/0142-9612(96)83289-3)
- Davis, J.R., 2004. *Handbook of thermal spray technology*, ASM Int. Materials; Park OH, USA.,
- Dental Board of California 1432. Howe Avenue• Sacramento, California. Future use of materials for dental restoration: WHO HQ, Geneva, Switzerland. *Material Properties Data: Alumina (Aluminum Oxide)*. https://www.drvales.com/storage/app/media/Dental_Materials_Fact_Sheet.pdf
- Dental Health Resource by Priya Grewal. 2016. <https://yourdentalhealthresource.com/top-ways-to-treat-tooth-decay-2/>
- Grujicic, M., C.L.Z.W.S. DeRosset, D. Helfrich, 2004. Adiabatic shear instability based mechanism for particles/substrate bonding in the coldgas dynamic-spray process. *Mater. Design*, 25: 681. <https://doi.org/10.1016/j.matdes.2004.03.008>
- Kashirin, A.I., O.F. Klyuev and T.V. Buzdygar. 2002. Apparatus for gas-dynamic coating, in U.S. Patent 6,402,050.
- King, P., M. Yandouzi and B. Jodoin. 2015. The physics of cold spray. *Modern Cold Spray*, pp. 31–72. https://doi.org/10.1007/978-3-319-16772-5_2
- Klinkov, S.V., Kosarev, V.F. and Rein, M., 2005. Cold spray deposition: Significance of particle impact phenomena. *Aerospace Sci. Technol.*, 9: <https://doi.org/10.1016/j.ast.2005.03.005>
- Kosarve, V.F., S.V. Klinkov, A.P. Alkhimov and A.N. Papyrin. 2001. On some aspects of gas dynamics of the cold spray process. *J. Therm. Spray Technol.*, 12: 265–281. <https://doi.org/10.1361/105996303770348384>
- Laudenbach, J., 2014. Common dental and periodontal evaluation and management. *The medical clinics of North America*. 98(6): 1239–1260. <https://doi.org/10.1016/j.mcna.2014.08.002>
- Li, W.Y., C. Zhang, C.J. Li and H. Liao. 2009. Modeling aspects of high velocity impact of particles in cold spraying by explicit finite element analysis. *J. Therm. Spray Technol.*,
- López-Píriz, R., L. Goyos-Ball, B. Cabal, S. Martínez, J.S. Moya, J.F. Bartolomé and R. Torrecillas. 2022. New ceramic multi-unit dental abutments with an antimicrobial glassy coating materials (Basel). 15(15): 5422. <https://doi.org/10.3390/ma15155422>
- Omar, N., M. Yamada, T. Yasui and M. Fukumoto. 2021. Bonding mechanism of cold-sprayed TiO₂ coatings on copper and aluminum substrates coatings 11(11): 1349. <https://doi.org/10.3390/coatings11111349>
- Papyrin, A., V. Kosarev, S. Klinkov, A. Alkhimov and V. Fomin. 2007. *Cold Spray Technology*.
- Schmidt, T., F.G. H. Assadi and H. Kreye. 2006. Development of a generalized parameter window for cold spray deposition. *Acta Mater.*, 54: 729–742. <https://doi.org/10.1016/j.actamat.2005.10.005>
- Singh, H., T.S. Sidhu and S.B.S. Kalsi. 2012. Cold spray technology: Future of coating deposition processes. *FRAC*, 22: 69–84. <https://doi.org/10.3221/IGF-ESIS.22.08>
- Spencer, K., V. Luzin and M. Zhang. 2010. Structure and properties of cold spray coatings, in *materials science forum*. pp. 4379–4394. <https://doi.org/10.4028/www.scientific.net/MSF.654-656.1880>
- Zeng, G., S.H. Zahiri, S. Gulizia, Y. Chen, C. Xu and X. Chen. 2020. Ivan Cole A comparative study of cell growth on a cold sprayed Ti-Ta composite. *J. Alloys Comp.*, 826: 154014. <https://doi.org/10.1016/j.jallcom.2020.154014>